ChemComm

Cite this: *Chem. Commun.*, 2011, **47**, 4700–4702

www.rsc.org/chemcomm

COMMUNICATION

New insight into the soot nanoparticles in a candle flame†

Zixue Su,[a] Wuzong Zhou*[a] and Yang Zhang[b]

Received 24th December 2010, Accepted 11th March 2011
DOI: 10.1039/c0cc05785a

Using anodic aluminium oxide films as collectors, all four well known carbon forms, diamond, graphitic, fullerenic and amorphous particles, are identified inside a candle flame, suggesting a new nucleation mechanism for diamond growth and fullerene formation in a combustion synthesizing process.

Candles have cast a light on man's progress for centuries not merely as a lighting source but also in the understanding of the fundamental combustion process. A candle flame with its fascinating lights, and mysterious and phantasmagoric inner structures, has been a research topic for about 400 years, from Francis Bacon's first combustion experiment by probing the candle flame structure in 1620 to Michael Faraday's series of lectures on the chemical history of a candle in 1860,[1] and to the investigation of flame characteristics at microgravity in the space shuttle and the Mir Station in recent years.[2] Unfortunately, the research of nanoparticles in candle flame is still difficult because the existing sampling methods[3–6] are either insensitive to the nanoparticles or unable to prevent the nanoparticles from further reaction.

A candle flame shows one of the most complex combustion processes due to its multiphasic nature and complex fuel compositions, C_nH_{2n+2} (n = 19 to 36), leading to rich carboneous structures in its heavy soot.[7,8] The study of soot formation and destruction mechanisms will be beneficial not only to the reduction of environmental pollution and improvement of combustion efficiency, but also to the nanoparticle growth through combustion synthesis, which is equally important and has received tremendous attention in recent years.[9] Soot formation in the combustion process has been investigated extensively in the past decades.[10–14] Analytical techniques including Raman spectroscopy and transmission electron microscopy (TEM) have greatly improved the knowledge about the structures of soot particles.[15–17] In the present work, a new sampling technique using ultrathin porous anodic aluminium oxide (AAO) foils to capture soot particles in a candle flame has been developed, followed by high resolution TEM (HRTEM) characterisation.

The AAO foils prepared *via* the typical two step anodisation have regular straight nanopores with tunable thickness and pore diameter.[18,19] The closed ends of the pores were opened by a treatment of phosphoric acid. When a foil (10 μm thin with 80 nm pore size) was inserted into a candle flame, its parallel channels allowed a passage of small particles (Fig. 1e). The disturbance of candle flame by AAO could be minimized by the high porosity and thinness of the foils.

All the sampling positions (Fig. 1b) were located near the flame axis. Due to the characteristic three-dimensional structure of candle flame, some soot particles at off-axis positions would also be collected when the foil was inserted. To reduce this effect, a small AAO foil was inserted through the periphery of the flame quickly and stayed at the target position for about 1 s then was removed quickly.

Although not all the particles in a flame can be filtered, we believe most small particles can pass through the AAO channels and the chain reactions of the combustion ceased. Consequently, these soot particles are in their original states at the collecting position. On the other hand, large particles deposited on the AAO surface as seen in Fig. 1(a) would undergo further reaction and aggregation.

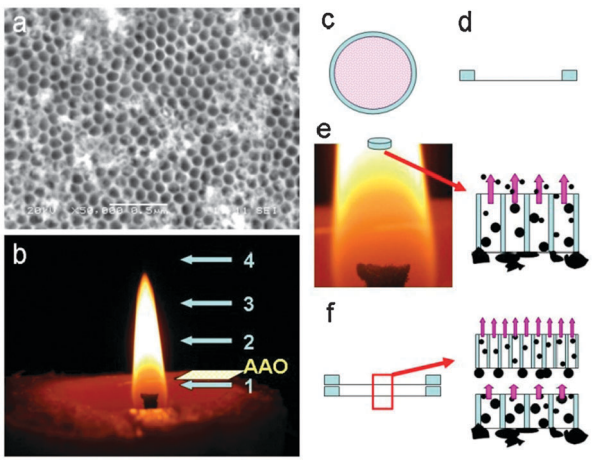

Fig. 1 (a) Top viewed SEM image of an AAO foil after collection of soot particles. Some small particles inside the pores are visible. (b) A candle flame. The inserting positions of the AAO foils are indicated: (1) lower, (2) centre, (3) upper, and (4) outer flame positions. Schematic drawing of (c) a top view and (d) a profile view of a single AAO foil supported on an aluminium ring. (e) A schematic drawing showing that only small soot particles move into the pores either being deposited on the inner surface of the pores or passing through the pores. (f) A schematic drawing of double-foil with different pore diameters and its filtering function of nanoparticles.

[a] *School of Chemistry, University of St Andrews, St Andrews, Fife, UK KY169ST. E-mail: wzhou@st-andrews.ac.uk*
[b] *Department of Mechanical Engineering, University of Sheffield, Sheffield, UK S1 3JD*

† Electronic supplementary information (ESI) available. See DOI: 10.1039/c0cc05785a

The small particles in the pores were recovered *via* an ultrasonic treatment. In addition, if a second AAO foil is placed on the top of the first one (Fig. 1f), smaller soot particles can also be collected by the second foil with a relatively slower rate. If we use such a double-foil with different pore sizes, *e.g.* 80 nm (bottom) and 40 nm (top), we are able to filter the soot particles and separate them according to their different sizes.

Fig. 2(a) is a typical TEM image of a large soot particle from the lower flame position. Enlarged TEM images show that it contains small chain-linked spherical particles of *ca.* 20 nm. The nanospherical particles contain many graphitic fragments with a typical d-spacing of 0.34 nm (Fig. 2b). In these nanospheres, some smaller graphitic spheres about 4 nm in diameter can be detected, indicating a multiple nucleation process. Many dark spots in a range of 2 to 4 nm in diameter were also detected, implying dense carbon particles, which have a diamond-like structure, although the crystal structures are heavily distorted (Fig. 2b).

The graphitic nanospheres grew larger when they moved to the centre flame position, approaching about 30 to 50 nm in diameter (Fig. 3a). The crystallinity of these spheres increased significantly to have an onion-like structure with a single core. In comparison with perfect onion-like graphitic structure where the graphitic layers are continuous and closed circles,[20] the graphitic layers in the nanospheres in Fig. 3(b) are broken into small fragments embedded in an amorphous phase.

Both the number and crystallinity of nanodiamond particles also increase. Most of them are in a range of 2 to 5 nm in size and separately embedded in the graphite spheres (Fig. 3b). Fig. 3(c) shows a typical nanodiamond particle with a diameter of *ca.* 3 nm, viewed down the [1$\bar{1}$0] zone axis. Both the measured d-spacings and the interplane angle match the diamond structure. It is noticed that the well known symmetry of diamond is not obvious in these nanodiamonds. In some crystallites, the (200) diffraction spots were not absent, indicating a possible symmetry of $F_{m\bar{3}m}$, which has been previously observed.[21] The present work suggests the lattice distortion may play an important role in this symmetry change.

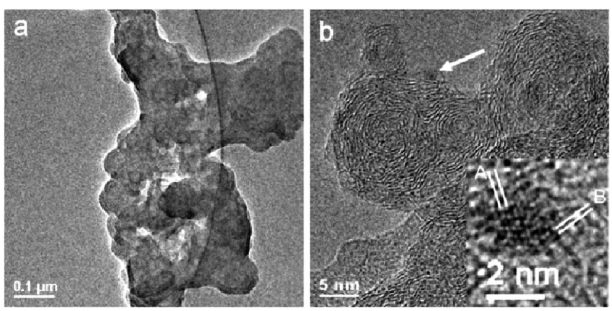

Fig. 2 TEM and HRTEM images of soot particles collected from the lower position of a candle flame. (a) A large soot particle containing connected small spheres. (b) HRTEM image of small particles showing coalescence of neighbouring particles and multi-nucleation of the graphitic particles. Some dark spots (one is indicated by an arrow) are higher density carbon particles. The inset is a typical HRTEM image of a dark spot showing a diamond structure, viewed down the [011] axis. The d-spacings of A and B (0.21 nm) with an interplane angle of 70.2° match the (111) planes in diamond.

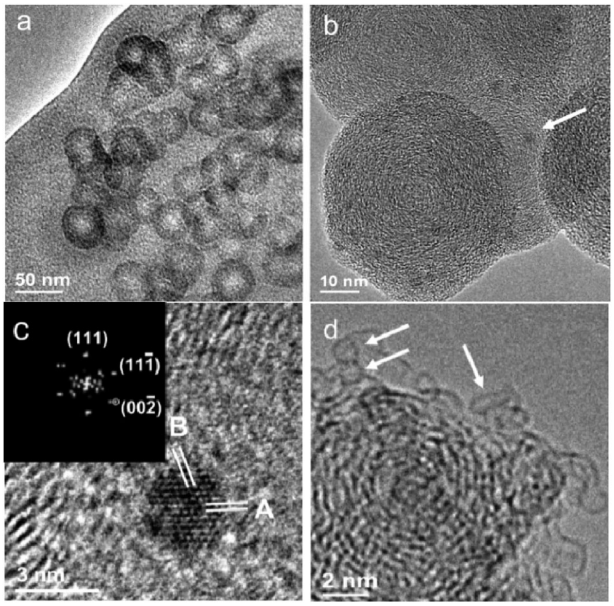

Fig. 3 TEM/HRTEM images of nanoparticle from the centre position of a candle flame, (a) spherical particles; (b) graphitic spheres with nanodiamond particles (one is indicated by an arrow); (c) a nanodiamond particle; (d) some fullerene particles as marked by the arrows. A and B in (c) indicate two atomic planes with d-spacings of 0.210 and 0.209 nm respectively, which can be indexed to two {111} planes of the diamond structure. The corresponding interplane angle is 110.18°. The inset is the corresponding FFT pattern.

The unit cell of diamond (a = 0.3567 nm) is very close to that of some metals. For example, copper has a face-centred cubic unit cell with a = 0.3608 nm. Several experiments were therefore performed in order to rule out any possible contaminations. First, no heavy elements were detected by EDX from candle wax and wick (Fig. S1). Second, no contaminates were detected from AAO foils before using (Fig. S2). Third, the number, size and crystallinity of the nanodiamond particles increased from lower flame to centre flame. Further changes in upper flame are discussed below.

Parallel experiments were performed for a natural gas flame using a Bunsen burner. It was found that fewer and smaller soot particles (<15 nm) were collected (Fig. S3a,b). A large number of the nanodiamond particles were observed again (Fig. S3c). These nanodiamond particles also contain defects or lattice distortion (Fig. S3d). The {200} diffraction spots are allowed, implying a symmetry of $F_{m\bar{3}m}$.

Diamond growth by chemical vapor deposition (CVD) has attracted great interest in the last decade.[22] However the nucleation mechanism of diamond from a gas phase was still unclear.[23,24] Although diamond nanoparticles[25] and diamond films[23] have been produced *via* combustion, the present work shows that 'live' nanodiamond particles can form inside a candle flame. This suggests that during the combustion flame CVD growth of diamond, the nucleation may take place in the flame before any carbon deposition on a hot substrate.

Another interesting result is the observation of fullerenes as shown in Fig. 3(d). The individual circles on the particle surface with a diameter in a range of 0.7 to 0.9 nm, matching the size of C_{60}, enable us to ensure the existence of fullerene in

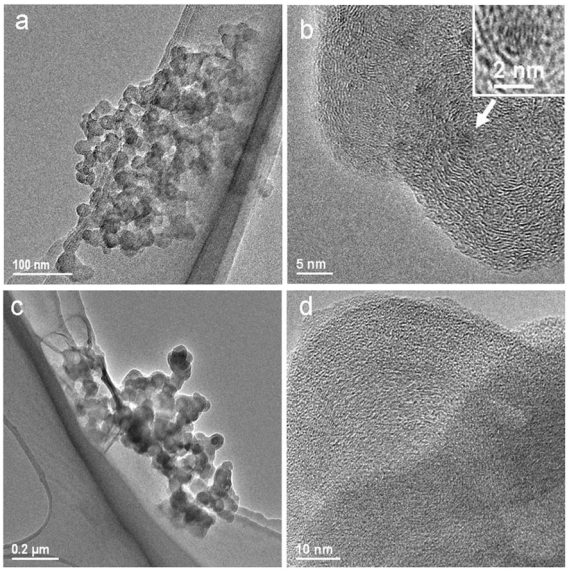

Fig. 4 (a) TEM and (b) HRTEM images of typical particles from upper position of a candle flame. The inset of (b) shows a structural image of a nanodiamond particle indicated by an arrow. (c) TEM and (d) HRTEM images of particles from outer flame.

the specimen. Some elongated fullerene particles (short nanotubes) were also found as indicated by an arrow on the right side of Fig. 3(d). The fullerenes were often observed on the surface of graphitic nanospheres, implying that they formed from a graphene-like single-layer carbon fragment which escaped from the surface of the nanospheres at a certain stage of combustion.

The graphitic nanospheres became smaller in upper flame and some particles coagulated with each other (Fig. 4a,b). The crystallinity was reduced significantly in comparison with those in centre flame. Both the number and the size of nanodiamond particles were reduced greatly. The particles collected from outer flame are further coagulated and mainly amorphous (Fig. 4c,d). Both the nanodiamond particles and graphite fragments were hardly observed.

Based on the microscopic observations of the soot particle transformation in a candle flame, we are now able to propose a more detailed combustion process. During the initial stage, long-chain hydrocarbons decompose to form C_2, C_3, C_2H_2, or other small radicals.[26] Six-membered aromatic rings then form from these radicals or directly from long-chain hydrocarbons due to their stability at high temperature.[27] In lower flame, a few planar polycyclic aromatic hydrocarbon molecules form a C–H containing graphitic fragment, which serves as a basic building unit for nanospheres. Meanwhile, some small radicals form dense carbon clusters and crystallise into nanodiamonds. Surface bonded hydrogen which remains from the hydrocarbon molecules contributes to the irregular shape of the nanodiamond particles, as previously reported,[28] with surface hydrogen, diamond, <3 nm in diameter, is energetically favoured over polycyclic aromatics without requiring the high pressures or extreme kinetic conditions.

When moving up to centre flame, crystallinity and size of soot particles increase. Fullerene particles were also found here, probably from graphene-like sheets on the nanosphere surface when the graphitic fragments were decomposed. No evidence supports the precursor role of fullerenes in soot particle formation as proposed previously.[29] Particle destruction dominates the process from centre to upper flame.

Candle flame has accompanied people for over 2000 years. We demonstrate that all four well known forms of carbon were detected at the same position in a candle flame. When we light a candle on a dinner table, over 1.5 million nanodiamond particles form in the flame per second, as estimated from our TEM observations. The newly developed sampling methodology using porous AAO foils will find its application for many combustion and nanoparticle synthetic processes. The present work may also open a new avenue for producing nanodiamond in a more economic and environmentally friendly way.

W.Z. appreciates EPSRC for PhD plus fellowship for Z.S.

Notes and references

1 M. Faraday, *Faraday's Chemical History of a Candle*, Chicago Review Press, Chicago, IL, USA, 1988.
2 D. L. Dietrich, H. D. Ross, Y. Shu, P. Chang and J. S. T'ien, *Combust. Sci. Technol.*, 2000, **156**, 1.
3 F. Ossler, S. E. Canton and J. Larsson, *Carbon*, 2009, **47**, 3498.
4 V. Krüger, C. Wahl, R. Hadef, K. P. Geigle, W. Stricker and M. Aigner, *Meas. Sci. Technol.*, 2005, **16**, 1477.
5 R. A. Dobbins and C. M. Megaridis, *Langmuir*, 1987, **3**, 254.
6 J. Cai, N. Lu and C. M. Sorensen, *Langmuir*, 1993, **9**, 2861.
7 D. Heymann, L. P. F. Chibante, R. R. Brooks, W. S. Wolbach and R. E. Smalley, *Science*, 1994, **265**, 645.
8 H. P. Liu, T. Ye and C. D. Mao, *Angew. Chem., Int. Ed.*, 2007, **46**, 6473.
9 A. Geol, P. Hebgen, J. B. V. Sande and J. B. Howard, *Carbon*, 2002, **40**, 177.
10 B. S. Haynes and H. G. Wagner, *Prog. Energy Combust. Sci.*, 1981, **7**, 229.
11 H. Richter and J. B. Howard, *Prog. Energy Combust. Sci.*, 2000, **26**, 565.
12 Z. A. Mansurov, *Combust., Explos. Shock Waves*, 2005, **41**, 727.
13 K. H. Homann, *Angew. Chem., Int. Ed.*, 1998, **37**, 2434.
14 K. H. Homann, *Combust. Flame*, 1967, **11**, 265.
15 A. Sadezky, H. Muckenhuber, H. Grothe, R. Niessner and U. Pöschl, *Carbon*, 2005, **43**, 1731.
16 M. Knauer, M. E. Schuster, D. S. Su, R. Schlögl, R. Niessner and N. P. Ivleva, *J. Phys. Chem. A*, 2009, **113**, 13871.
17 J. O. Müller, D. S. Su, U. Wild and R. Schlögl, *Phys. Chem. Chem. Phys.*, 2007, **9**, 4018.
18 Z. X. Su and W. Z. Zhou, *Adv. Mater.*, 2008, **20**, 3663.
19 Z. X. Su, G. Hahner and W. Z. Zhou, *J. Mater. Chem.*, 2008, **18**, 5787.
20 F. Banhart, J. C. Charlier and P. M. Ajayan, *Phys. Rev. Lett.*, 2000, **84**, 686.
21 G. Murrieta, A. Tapia and R. de Coss, *Carbon*, 2004, **42**, 771.
22 S. T. Lee, Z. D. Lin and X. Jiang, *Mater. Sci. Eng., R*, 1999, **25**, 123.
23 B. Atakan, K. Lummer and K. K. Höinghaus, *Phys. Chem. Chem. Phys.*, 1999, **1**, 3151.
24 S. T. Lee, H. Y. Peng, X. T. Zhou, N. Wang, C. S. Lee, I. Bello and Y. Lifshitz, *Science*, 2000, **287**, 104.
25 W. A. Carrigton, L. M. Hanssen, K. A. Snail, D. B. Oakes and J. E. Butler, *Metall. Trans. A*, 1989, **20**, 1282.
26 A. Kossiakoff and F. O. Rice, *J. Am. Chem. Soc.*, 1943, **65**, 590.
27 S. E. Stein and A. Fahr, *J. Phys. Chem.*, 1985, **89**, 3714.
28 P. Badziag, W. S. Verwoerd, W. P. Ellis and N. R. Greiner, *Nature*, 1990, **343**, 244.
29 Q. L. Zhang, S. C. O'Brien, J. R. Heath, Y. Liu, R. F. Curl, H. W. Kroto and R. E. Smalley, *J. Phys. Chem.*, 1986, **90**, 525.

